Epitaxial lateral overgrowth of *c*-plane α-Ga_2O_3 using a stripe mask with ultra-narrow windows

Yuichi Oshima[1]* and Takashi Shinohe[2]

[1]*Research Center for Electronic and Optical Materials, National Institute for Materials Science, 1-1 Namiki 305-0044, Tsukuba, Japan*

[2]*FLOSFIA, Inc, 1-29 Goryoohara, Nishikyo-ku 615-8245, Kyoto, Japan*

*E-mail: OSHIMA.Yuichi@nims.go.jp

We demonstrated the epitaxial lateral overgrowth of α-Ga_2O_3 by halide vapor phase epitaxy using a stripe mask with an ultra-narrow window width of 50–750 nm. α-Ga_2O_3 stripes were formed only on the windows without unintentional nucleation on the mask, even on the mask with the narrowest window. Etch pit observations and cross-sectional TEM revealed that the propagation of dislocations into the regrown α-Ga_2O_3 was dramatically reduced by narrowing the window. The overall dislocation density in the coalesced film, including the window region and coalesced boundaries, was as low as 4×10^7 cm^{-2} in the case of the 50-nm-window mask. We believe these results strongly contribute to the realization of α-Ga_2O_3-based high-performance future power devices.

Corundum-structured α-Ga_2O_3 is a metastable polymorph of Ga_2O_3[1–3] and exhibits the largest bandgap (E_g = 5.2–5.3 eV [4,5]) among the Ga_2O_3 polymorphs. In addition, α-Ga_2O_3 can form solid solutions with other corundum-structured oxides such as α-$(AlGa)_2O_3$, offering a large degree of freedom in band engineering.[6,7] Furthermore, isomorphic *p*-type oxides with relatively small lattice mismatches, such as α-$(IrGa)_2O_3$, can form hetero-*pn* junctions.[8–10] Thus, α-Ga_2O_3 is a promising material for future power device applications. Indeed, promising device prototypes, such as Schottky barrier diodes (SBDs) with very-low on-resistance of 0.1 mΩcm^2,[11] ampere-class SBDs with a breakdown voltage (V_B) of 1.7 kV,[12] low-leakage junction-barrier controlled SBDs using hetero-*pn* junctions,[12] normally-off operation metal oxide semiconductor field effect transistors (MOSFETs) with a *p*-well layer, [13] and MOSFETs with a V_B of 2.3 kV[14] have been reported.

As bulk α-Ga_2O_3 substrates are not available, α-Ga_2O_3 is grown hetero-epitaxially. Isomorphic sapphire is usually used as a substrate because large-diameter high-quality wafers are available at a reasonable price. Various film growth techniques, such as mist-CVD[4,9], halide vapor-phase epitaxy (HVPE) [5,15], molecular bean epitaxy[16,17], metal-organic vapor-phase epitaxy[18], and atomic layer deposition,[19] are available. However, the dislocation density in conventional α-Ga_2O_3 films is typically as high as ~10^{10} cm^{-2} because of the large lattice mismatch ($\Delta a/a$ ~ 4.5%, $\Delta c/c$ ~ 3.3%).[20,21] Such a high dislocation density significantly scatters carriers, decreasing electron mobility.[22] Theoretical calculations have predicted that the influence of dislocations should be negligible when the density is of the order of 10^7 cm^{-2} or less.[23]

Epitaxial lateral overgrowth (ELO) is an effective method for decreasing the dislocation density.[20,24–27] In the ELO process, α-Ga_2O_3 is regrown on an α-Ga_2O_3 seed layer (or sometimes directly on a sapphire substrate) covered by a patterned dielectric

mask, such as SiO_2 or TiO_2. The stripe pattern of these masks is the most frequently used. The reported widths of the window and mask (*W* and *M*, respectively) are typically on the micrometer scale. During the regrowth process, α-Ga_2O_3 selectively nucleate on the windows. Then the α-Ga_2O_3 stripes grow vertically and laterally to form a coalesced compact film. In the laterally grown area on the mask, the dislocation density drastically decreases to 10^6–10^7 cm^{-2} (except for the coalesced boundary) because the dislocations in the seed layer are blocked by the mask. However, in the window area, the dislocation density remains similar to that in the seed layer because the dislocations in the seed layer propagate directly into the regrown α-Ga_2O_3. For example, when the widths of the window and mask are the same, the overall dislocation density decreases by a factor of only 0.5, even if the dislocation density in the laterally grown area, including the coalesced boundary, was zero. The residual defective area is a major problem in the ELO technique and is not limited to α-Ga_2O_3.

To solve this problem, some effective methods have been developed for GaN, such as inclined-faceted growth, which enhances the bending of dislocations to minimize the elastic energy, [28–32] and thick film growth, which disperses the dislocations.[33] Notably, thick film growth is also effective in decreasing the dislocation density because of the pair annihilation of dislocations with Burgers vectors of opposite signs. These methods have also been applied to α-Ga_2O_3.[20,24,34] For example, a uniform dislocation density of 1.1×10^7 cm^{-2} was reported for α-Ga_2O_3 as a result of thick film growth with faceted surfaces combined with conventional ELO, although a very thick film growth of 140 μm was necessary.[34] If these methods are combined with ELO using a mask pattern with a much smaller fill factor (a small fraction of the window area), which should provide a small fraction of the defective area, further reduction in the dislocation density is expected.

However, it would be problematic to merely increase *M* to decrease the fill factor because a thicker film growth is required to achieve coalescence. There is also a risk of undesired nucleation on the mask if *M* is greater than the surface diffusion length of the growth species. On the other hand, it is a good strategy to decrease *W* while maintaining a moderate value of *M*. However, the reported *W* remained on the micrometer scale because of the limited spatial resolution of photolithography. In this study, we used electron-beam (EB) lithography to reduce *W* beyond this limitation, and demonstrated the ELO of α-Ga_2O_3 using a mask that was fabricated by EB lithography.

First, we prepared a *c*-plane α-Ga_2O_3/sapphire template with a SiO_2 stripe mask along $[1\bar{1}00]$ on top. The α-Ga_2O_3 seed layer (2-μm thick) was grown using HVPE. Growth was allowed to proceed in a horizontal quartz reactor at 520 °C under atmospheric pressure using O_2 (>99.99995% pure) and GaCl as growth precursors. GaCl was synthesized in situ upstream of the reactor via the chemical reaction of Ga (>99.99999% pure) and HCl gas (>99.999% pure). In addition to the growth precursors, HCl gas was supplied separately to the growth zone to suppress parasitic gas-phase reactions.[35] GaCl/O_2/HCl was supplied at partial pressures of 0.125, 1.25, and 0.125 kPa. N_2 (dew point < –110 °C) was used as the carrier gas. The growth rate of flat *c*-plane α-Ga_2O_3 was 14 μm/h under these growth conditions.

The SiO_2 mask was fabricated using EB lithography. A SiO_2 layer (50-nm thick) was deposited by RF sputtering. Window width *W* was 50–750 nm, and mask width *M* was 5 μm. For comparison, a stripe mask with *W*/*M* = 3 μm/ 7 μm was prepared using conventional photolithography.

α-Ga_2O_3 was then regrown on the masked template using the same HVPE reactor and growth conditions for 5–90 min.

The morphology of the regrown α-Ga_2O_3 was observed by scanning electron microscopy (SEM). The dislocations were visualized as etch pits on the surface using HCl gas etching,[36] and were observed by SEM to clarify the distribution and estimate the density. The dislocation behavior was observed by cross-sectional bright-field transmission electron microscopy (TEM).

Figure 1 (a)–(c) show the SEM images of the samples grown for 2–15 min using the mask with the narrowest window width. An α-Ga_2O_3 stripe was selectively formed on the window without any nucleation of unintentional α-Ga_2O_3 grains on the mask. The α-Ga_2O_3 stripes exhibited a *c*-plane top surface and *a*-plane sidewalls even at the very early stages of growth, and these facets were preserved until coalescence.

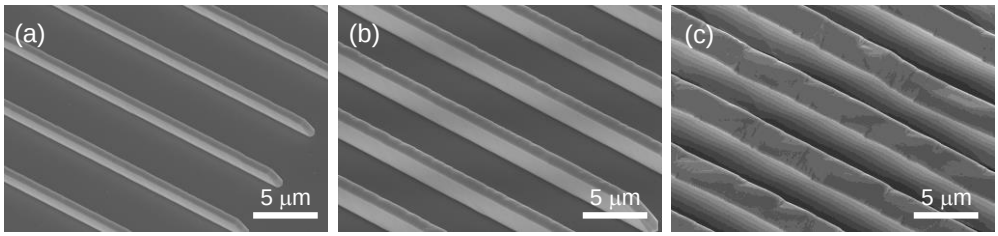

Figure 1. Bird's-eye-view SEM images of α-Ga_2O_3 samples grown for (a) 2 min, (b) 5 min, and (c) 15 min using the stripe mask with W/M = 50 nm/5 μm.

Figures 2(a)–(c) show SEM images of the α-Ga_2O_3 stripes grown for 60 min. Using mask patterns with various window widths *W*, dislocations exposed on the surface were visible as etch pits along the central axis of each α-Ga_2O_3 stripe. The number of dislocations effectively decreased with decreasing *W*.

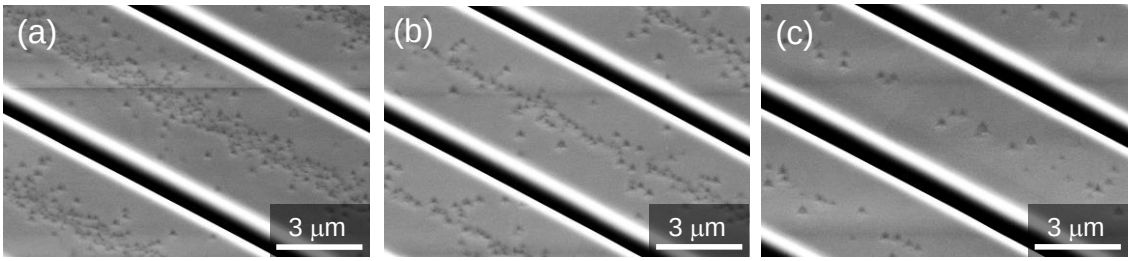

Figure 2. Bird's-eye-view SEM images of the ELO α-Ga_2O_3 samples grown for 60 min using the stripe masks with (a) *W*/*M* = 750 nm/5 μm, (b) *W*/*M* = 250 nm/5 μm, and *W*/*M* = 50 nm/5 μm.

We performed cross-sectional TEM of the sample grown in the narrowest window (*W*/*M* = 50 nm/ 5 μm) to clarify the dislocation behavior. Figure 3(a) shows the cross-sectional shape of the sample and observed areas. The height from the regrowth interface to the top surface was approximately 23 μm, which was significantly larger than that expected from the growth rate of a plain film. This is probably due to the contribution of precursors that were not consumed on the mask. The height of the coalesced part was 17 μm, and the top part did not coalesce. Figures 3(b) and (c) show the TEM images observed from the *m*-axis in the vicinity of the regrowth interface and top surface, respectively. Figure 3(d) shows a higher-magnification TEM image of the region around the window. It should be noted that the TEM specimen was taken from a different area than that used for Fig. 3(b). A cross-sectional TEM image of an α-Ga_2O_3 stripe grown using a conventional stripe mask (*W*/*M* = 3 μm / 7 μm) is shown for comparison (Figure 3(e)). TEM observations clarified that dislocations propagated into

the regrown α-Ga_2O_3 through the 50-nm window, and extended toward the top surface, similar to the conventional case. However, the number of propagated dislocations was significantly reduced. The formation of dislocations can be observed along the coalesced boundary, as is typically observed in conventional ELO films. In this study, we did not perform a detailed analysis of dislocation character; such investigation should be addressed in future work.

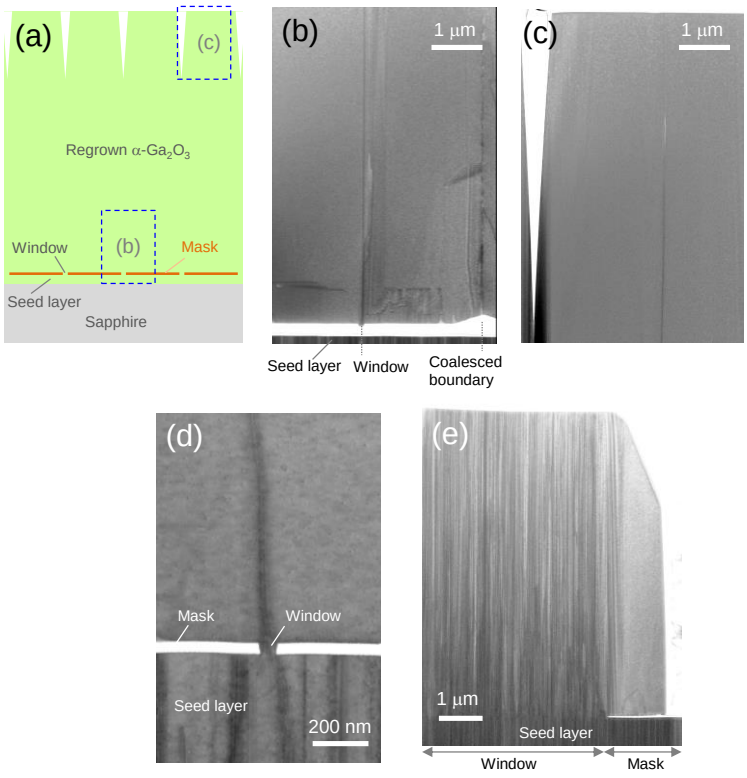

Figure 3. (a) A cross-sectional schematic of the partially coalesced ELO α-Ga_2O_3 sample grown for 60 min using the stripe mask with *W*/*M* = 50 nm/5 μm. (b), (c) Cross-sectional TEM images observed from the *m*-direction at positions indicated in (a). the regrown α-Ga_2O_3 was separated from the seed layer in the sampling process probably because of residual strain. (d) A higher magnification TEM image around the window. (e) A cross-sectional TEM image of an α-Ga_2O_3 stripe grown on the conventional stripe mask with *W*/*M* = 3 μm /7 μm.

Figure 4(a) shows the SEM images of the fully coalesced ELO α-Ga_2O_3 sample grown for 90 min using the stripe mask with the narrowest window. For comparison, a SEM image of a conventional sample prepared by using the same HVPE growth recipe

is shown in Figure 4(b). The dislocations were visualized as etch pits using HCl gas etching. In the case of the conventional sample, a broad high-dislocation-density area remained on the windows, while a high-quality area was observed on the mask. Therefore, the overall dislocation density was comparable to that of the seed layer. However, in the narrow-window sample, the number of dislocations in the window drastically decreased, as confirmed by cross-sectional TEM. Although a line of dislocations was observed along the coalesced boundary, as in the conventional case, the overall dislocation was as low as 4×10^7 cm^{-2}.

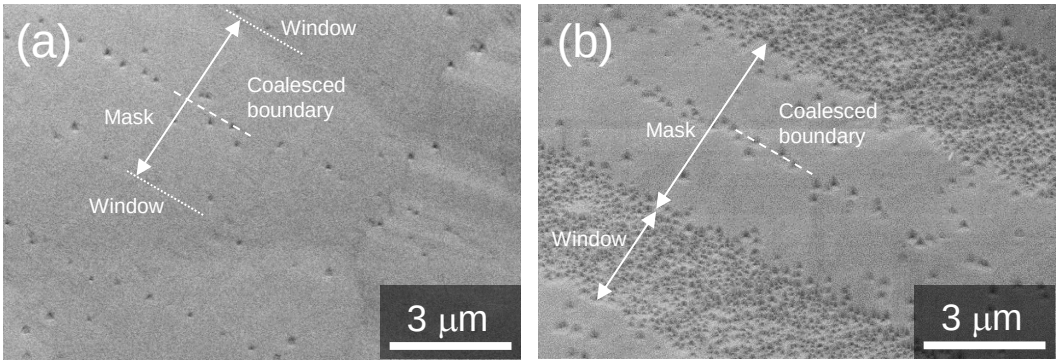

Figure 4. Bird's-eye-view SEM images of fully coalesced samples grown for 90 min on the stripe mask with (a) *W*/*M* = 50 nm/5μm and (b) *W*/*M* = 3 μm /7 μm

We demonstrated the ELO of α-Ga_2O_3 using a stripe mask with a very narrow window width (50–750 nm) fabricated using EB lithography. During the regrowth process, the α-Ga_2O_3 stripes selectively nucleated on the window, even for the narrowest window. Etch pit observations and cross-sectional TEM revealed that the number of dislocations along the central axis of each α-Ga_2O_3 stripe was drastically reduced by narrowing the window. The α-Ga_2O_3 stripes grew vertically and laterally to coalesce, forming a compact film. The overall dislocation density was as low as 4×10^7 cm^{-2}, while the dislocation density in a conventional ELO film remained comparable to that in the seed layer owing to the large fraction of the defective area. We believe this

technique, which enables the fabrication of a high-quality α-Ga_2O_3 epitaxial film without highly defective areas, will strongly push the realization of α-Ga_2O_3-based high-performance future power devices.

Acknowledgments

This work was supported by the Innovative Science and Technology Initiative for Security (Grant Number JPJ004596), ATLA, Japan. This work was also supported by the "Advanced Research Infrastructure for Materials and Nanotechnology in Japan (ARIM)" initiative of the Ministry of Education, Culture, Sports, Science, and Technology (MEXT) under Proposal Number JPMXP1224NM5455.

REFERENCES

[1] R. Roy, V. G. Hill and E. F. Osborn, J. Am. Chem. Soc. **74**, 719 (1952).

[2] H. Y. Playford, A. C. Hannon, E. R. Barney and R. I. Walton, Chemistry - A European Journal **19**, 2803 (2013).

[3] I. Cora, F. Mezzadri, F. Boschi, M. Bosi, M. Čaplovičová, G. Calestani, I. Dódony, B. Pécz and R. Fornari, Cryst. Eng. Comm. **19**, 1509 (2017).

[4] D. Shinohara and S. Fujita, Jpn. J. Appl. Phys. **47**, 7311 (2008).

[5] Y. Oshima, E. G. Víllora and K. Shimamura, Appl. Phys. Express **8**, 055501 (2015).

[6] H. Ito, K. Kaneko and S. Fujita, Jpn. J. Appl. Phys. **51**, 100207 (2012).

[7] S. Fujita and K. Kaneko, J. Cryst. Growth **401**, 588 (2014).

[8] S. Kan, S. Takemoto, K. Kaneko, I. Takahashi, M. Sugimoto, T. Shinohe and S. Fujita, Appl. Phys. Lett. **113**, 212104 (2018).

[9] K. Kaneko, S. Fujita and T. Hitora, Jpn. J. Appl. Phys. **57**, 02CB18 (2018).

[10] K. Kaneko, Y. Masuda, S. I. Kan, I. Takahashi, Y. Kato, T. Shinohe and S. Fujita, Appl. Phys. Lett. **118,** 102104 (2021).

[11] M. Oda, R. Tokuda, H. Kambara, T. Tanikawa, T. Sasaki and T. Hitora, Applied Physics Express **9**, 021101 (2016).

[12] T. Shinohe, in *2024 IEEE International Meeting for Future of Electron Devices, Kansai (IMFEDK)* (IEEE, 2024) pp. 1. [doi:10.1109/IMFEDK64776.2024.10814202]

[13] T. Shinohe, in *2022 International Power Electronics Conference (IPEC-Himeji 2022-ECCE Asia)* (IEEE, 2022) pp. 627. [doi: 10.23919/IPEC-Himeji2022-ECCE53331.2022.9807052]

[14] Y. J. Jeong, J. H. Park, M. J. Yeom, I. Kang, J. Y. Yang, H. Y. Kim, D. W. Jeon and G. Yoo, Applied Physics Express **15**, 074001 (2022).

[15] D. W. Jeon, H. Son, J. Hwang, A. Y. Polyakov, N. B. Smirnov, I. V. Shchemerov, A. V. Chernykh, A. I. Kochkova, S. J. Pearton and I. H. Lee, APL Mater. **6**, 121110 (2018).

[16] Z. Cheng, M. Hanke, P. Vogt, O. Bierwagen and A. Trampert, Appl. Phys. Lett. **111**, 162104 (2017).

[17] R. Jinno, C. S. Chang, T. Onuma, Y. Cho, S.-T. Ho, D. Rowe, M. C. Cao, K. Lee, V. Protasenko, D. G. Schlom, D. A. Muller, H. G. Xing and D. Jena, Sci. Adv. **7**, eabd5891 (2021).

[18] A. F. M. A. U. Bhuiyan, Z. Feng, H. L. Huang, L. Meng, J. Hwang and H. Zhao, APL Mater. **9**, 101109 (2021).

[19] J. W. Roberts, J. C. Jarman, D. N. Johnstone, P. A. Midgley, P. R. Chalker, R. A. Oliver and F. C. P. Massabuau, J. Cryst. Growth **487**, 23 (2018).

[20] Y. Oshima, K. Kawara, T. Shinohe, T. Hitora, M. Kasu and S. Fujita, APL Mater. **7**, 022503 (2019).

[21] H. Takane, S. Konishi, Y. Hayasaka, R. Ota, T. Wakamatsu, Y. Isobe, K. Kaneko and K. Tanaka, J. Appl. Phys. **136**, 025105 (2024).

[22] H. Son, Y. Choi, J.-H. Park, B. Ryu and D.-W. Jeon, ECS Journal of Solid State Science and Technology **9**, 055005 (2020).

[23] H. Takane, H. Izumi, H. Hojo, T. Wakamatsu, K. Tanaka and K. Kaneko, J. Mater. Res. **38**, 2645 (2023).

[24] Y. Oshima, K. Kawara, T. Oshima, M. Okigawa and T. Shinohe, Jpn. J. Appl. Phys. **59**, 025512 (2020).

[25] K. Kawara, Y. Oshima, M. Okigawa and T. Shinohe, Appl. Phys. Express **13**, 075507 (2020).

[26] R. Jinno, N. Yoshimura, K. Kaneko and S. Fujita, Jpn. J. Appl. Phys. **58**, 120912 (2019).

[27] G. T. Dang, T. Yasuoka and T. Kawaharamura, Appl. Phys. Lett. **119**, 041902 (2021).

[28] A. Usui, H. Sunakawa, A. Sakai and A. A. Yamaguchi, Jpn. J. Appl. Phys. **36** L899 (1997).

[29] K. Hiramatsu, K. Nishiyama, M. Onishi, H. Mizutani, M. Narukawa, A. Motogaito, H. Miyake, Y. Iyechika and T. Maeda, J. Cryst. Growth **221**, 316 (2000).

[30] Y. Oshima, T. Eri, M. Shibata, H. Sunakawa and K. Kobayashi, Jpn. J. Appl. Phys. Vol. **42**, L1 (2003).

[31] K. Motoki, T. Okahisa, R. Hirota, S. Nakahata, K. Uematsu and N. Matsumoto, J. Cryst. Growth. **305**, 377 (2007).

[32] T. Yoshida and M. Shibata, Jpn. J. Appl. Phys. **59**, 071007 (2020).

[33] K. Fujito, S. Kubo, H. Nagaoka, T. Mochizuki, H. Namita and S. Nagao, J. Cryst. Growth **311**, 3011 (2009).

[34] Y. Oshima, H. Ando and T. Shinohe, Appl. Phys. Express **16**, 065501 (2023).

[35] Y. Oshima, K. Kawara, T. Oshima, M. Okigawa and T. Shinohe, Semicond. Sci. Technol **35**, 055022 (2020).

[36] Y. Oshima, S. Yagyu and T. Shinohe, J. Cryst. Growth **576**, 126387 (2021).